DERIVING CLOUD MOTION VECTORS FROM A PV POWER PLANT ON-SITE SENSORS

Juan L. Bosch
Jan Kleissl
Department of Mechanical and Aerospace Engineering
Center for Renewable Resources and Integration
University of California, San Diego
La Jolla, California 92093-0411
jlbosch@ucsd.edu
jkleissl@ucsd.edu

ABSTRACT

Advancing to a high photovoltaic penetration scenario implies a good understanding of both the spatial and temporal patterns of the solar energy input. Shadowing induced by clouds is the main source of the short-term fluctuations in the produced power.

Cloud speed is one input needed for most of the forecasting and nowcasting approaches, however its measure at a local scale is still an unsolved challenge. The main goal of this study is to estimate the cloud motion vector (CMV) using existing sensors at a 48 MW PV plant located in Henderson, Nevada. Data was acquired during 1 year with 1 second resolution for both the five reference cells and 96 power inverters.

CMVs are calculated assuming a linear cloud shadow edge (LCE) passing through three unaligned sensors. A different method is applied to the 96 power inverters dataset. This second method is used to validate cloud speeds and is based on the signal correlation between two sensors aligned with the cloud direction. Our analysis shows good agreement between both methods.

1. INTRODUCTION

Solar photovoltaic (PV) power output variability caused by clouds is a major barrier to expansion of solar power (e.g. (1)). Cloud velocity is a principal input to most short-term forecast (2,3) and variability models (4,5). In simple terms for a cloud passage, the ramp magnitude depends on the cloud optical depth; in addition the ramp rate is a function of how long it takes for a cloud to cover the plant. CMVs have traditionally been obtained from satellite imagery (6-8) by tracking a feature in successive images. However, not only are satellite data complex to acquire and process, but infrequent data update (every 15 to 30 min) and data transfer delays also may not allow detection of mesoscale convective clouds in a timely manner. Consequently, local ground measurements of cloud speed are advantageous for short-term solar variability and solar forecasting.

The main goal in this study is to estimate cloud speed without additional instrumentation using time delays in cloud arrival times detected using triplets of reference cells and inverter output of a solar power plant. The principal assumption is that the cloud edge shadow can be considered linear and cloud speed constant as the cloud passes over the triplet.

Previous work by Bosch et al. (9) covered a special case of sensors arranged orthogonally, equidistant, and in close proximity to the origin. CMV detection required fast data sampling rates and the validation was limited to four days. The conditions on the sensors set up in the present paper are less restrictive and results are validated with a year of data.

2. DATA

Plane of Array irradiance I_{POA} was measured using five reference cells at the Sempra US Gas & Power Copper Mountain 48 MW PV Plant (Latitude 35.78° ; Longitude -115.00 °) with a sampling of 1s. The reference cells are oriented towards south and with a tilt angle of 25°. The selected cells are shown in Fig. 1 and combined in two different triplets as shown in Table 1.

Fig. 1: Power plant layout showing the selected reference cells. White boxes near the 'aisles' of the panel blocks correspond to inverter locations.

TABLE 1: DESCRIPTION OF THE TWO TRIPLETS. CONSULT FIG. 1 FOR SENSOR NUMBERS AND VARIABLES NAMES ARE DEFINED IN FIG. 2.

Triplet	T1	T2
Sensor o	1	5
Sensor A	2	4
Sensor B	3	3
α_0 [^{o}]	-3.2	+1.5
θ [^{o}]	-36.0	+36.7
d_A [m]	284	283
d_B [m]	365	360

Other reference cells can be found in the site, but they were not selected due to their larger spacing (520 m and more). Table 1 shows the distances and angles found in the selected triplets. In addition, power output from the 96 inverters located at the plant were used to validate the cloud speed results obtained from the reference cell triplets. This second set of data was also acquired at 1 s temporal resolution and has a typical uncertainty of 1-2%. Other specifications and model names are not shown due to confidentiality of the data.

3. METHODS

3.1 Linear Cloud Edge (LCE)

Let us consider a triplet of sensors *o*, *A* and *B*, placed in known arbitrary positions (Fig. 2). For simplicity, we will consider the sensor *o* as the origin of the coordinate system, and the *x* axis to be aligned with the $\overline{oA}$ direction.
A sample cloud edge passing through the array is shown in Fig. 3 using the defined coordinate system. We define the time needed for the cloud to move from C_A to *A* (t_A) and from C_B to *B*, (t_B). The cloud motion direction is given by either the lines $\overline{BC_B}$, $\overline{C_A A}$ or the motion vector ***v***. Equations 1-8 show the steps to calculate the CMV.

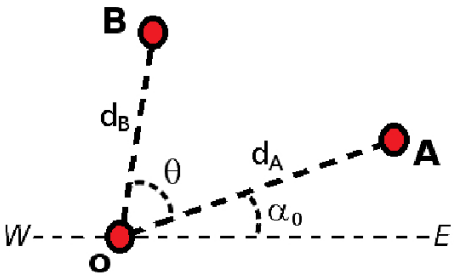

Fig. 2: Arbitrary triplet of sensors where α_0 is the angle between the West-East direction and the line $\overline{oA}$, and θ is the angle between the two pairs of sensors $\overline{oA}$ and $\overline{oB}$. The distances from sensor o to sensors A and B are given by d_A and d_B respectively.

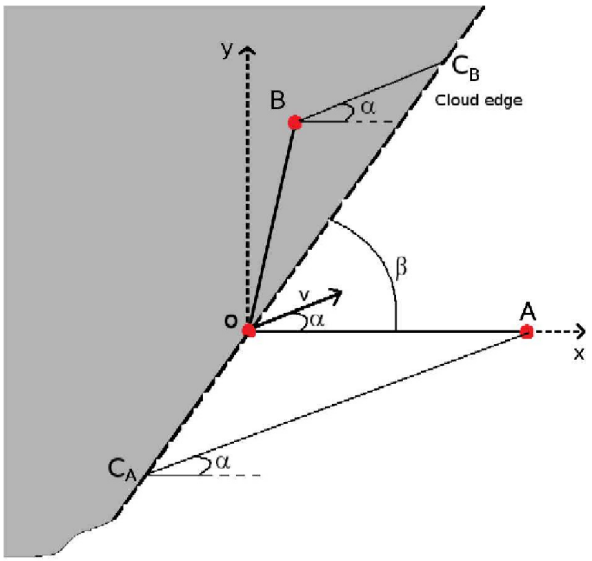

Fig. 3: Schematic of a linear cloud edge passing a sensor triplet. β is the angle between the cloud edge and the *x* axis, and α is the angle between the CMV ***v*** and the *x* axis. C_A and C_B are the cloud edge points that pass over sensors *A* and *B*, respectively.

The main vectors in Fig. 3 can be expressed as:

$$\begin{aligned} \mathbf{v} &= (v\cos\alpha, v\sin\alpha) \\ \mathbf{r_o} &= (0,0) \\ \mathbf{r_A} &= (d_A, 0) \\ \mathbf{r_B} &= (d_B\cos\theta, d_B\sin\theta) \\ \mathbf{r_{C_A}} &= \overline{oC_A}\hat{\mathbf{c}} \\ \mathbf{r_{C_B}} &= \overline{oC_B}\hat{\mathbf{c}} \\ \hat{\mathbf{c}} &= (\cos\beta, \sin\beta) \end{aligned} \qquad \text{Eq.1}$$

Where $\hat{\mathbf{c}}$ is an unitary vector in the direction of the cloud edge.

Basic kinematic equations can be used to reach the analytic expressions for t_A and t_B

$$\begin{aligned} \mathbf{r_A} &= \mathbf{r_{C_A}} + t_A\mathbf{v} \\ \mathbf{r_B} &= \mathbf{r_{C_B}} + t_B\mathbf{v} \end{aligned} \quad \text{Eq. 2}$$

Applying the cross product with $\hat{\boldsymbol{c}}$:

$$t_A = \frac{\mathbf{r_A} \times \hat{\mathbf{c}}}{\mathbf{v} \times \hat{\mathbf{c}}} \quad \text{Eq. 3}$$

$$t_B = \frac{\mathbf{r_B} \times \hat{\mathbf{c}}}{\mathbf{v} \times \hat{\mathbf{c}}} \quad \text{Eq. 4}$$

In general, it can be deduced from Eqs. 3-4 that if a sensor pair is parallel to the cloud edge, the shadow will reach both sensors at the same time simplifying the problem. For example, if sensors *o* and *B* are parallel to the cloud edge, then t_B will be 0 and β will be equal to θ. On the other hand, if the cloud motion vector is parallel to the cloud edge, the shadow will always be on the origin and never reach the other sensors.

Defining the vectors $\mathbf{v_A}$ and $\mathbf{v_B}$

$$\begin{aligned} \mathbf{v_A} &= \mathbf{r_A}/t_A \\ \mathbf{v_B} &= \mathbf{r_B}/t_B \end{aligned} \quad \text{Eq. 5}$$

Eq. 2 can be rewritten as:

$$\begin{aligned} \mathbf{v_A} \times \hat{\mathbf{c}} &= \mathbf{v} \times \hat{\mathbf{c}} \\ \mathbf{v_B} \times \hat{\mathbf{c}} &= \mathbf{v} \times \hat{\mathbf{c}} \end{aligned} \quad \text{Eq. 6}$$

Solving Eq. 6 yields

$$\frac{-v\sin\alpha}{v_A - v\cos\alpha} = \frac{-v_B\sin\theta}{v_A - v_B\cos\theta} \quad \text{Eq. 7}$$

Since the time lags t_A and t_B can be obtained from the measurements and the sensor locations are known, we are left with two unknowns (α and v), and one equation (Eq. 7). Assigning the indices 1 and 2 for the first and second cloud passage, respectively, leads to Eq. 8

$$\alpha = \arctan\left[\frac{-d_B\sin\theta\ (t_{A1} - t_{A2})}{d_A\ (t_{B1} - t_{B2}) - d_B\cos\theta\ (t_{A1} - t_{A2})}\right] \quad \text{Eq. 8}$$

Once α is obtained from Eq. 8, v can be calculated using Eq. 7.

The final step to obtain the cloud cardinal direction is to apply the α_0 rotation defined in Fig. 2 to the calculated α. t_A and t_B are determined from the timing of local maxima and minima of the measured I_{POA}. The maxima can occur when cloud enhancement causes an increase in I_{POA} just before of after a cloud shades the sensors, while minima in I_{POA} occur near the cloud center. More often, maxima and minima occur during the shading event due to variability in intra-cloud opacity. Time lags between the maxima and minima observed at different sensor locations yield t_A and t_B for particular cloud events.

Following the quality control process described in (9), the final set of CMV derived from the LCE method is reduced. An additional quality control is performed applying a mode filter with a 1-hour window to the final set. The next step is to compare the results with those obtained with a second method described in section 3.2.

3.2 Cross-Correlation Method (CCM)

The basic premise is that for a pair of sensors aligned with the cloud motion, separated by a distance *D*, their irradiances are highly correlated, but with a time lag *t*. Once the lag has been determined (e.g. by analyzing the signal cross correlation), cloud speed can be calculated as $v=D/t$.

Previous results from a sensor array in a semi-circle with diameter 12 m (9) show that both methods yield similar values for CMV direction, and this study will use the CCM as a validation for the LCE results. After quality control has been applied to the LCE results, a pair of inverters aligned with the LCE cloud direction is used to obtain the MCC cloud speed.

The 96 inverters combinations cover the whole range of possible directions, but with different separation distances. The most aligned pairs are preselected from the initial set of 2^{96} pairs. From the most aligned pairs, one with a separation distance close to 500m is selected and used for the CCM cloud speed algorithm. Finally, the correlation coefficient *R* obtained is checked for quality control discarding the cloud speeds with R <0.78.

4. RESULTS

After discarding the completely clear days, the LCE method was used on the remaining 226 days to obtain pairs of cloud speed and direction. Following the procedure in Section 3.2 the MCC method was applied and cloud speed was calculated independently.

The year was split into four seasons to study the seasonal variation of the model performance. The periods considered are Q1 (January-March 2012, winter frontal systems), Q2 (April-June 2012, mostly clear), Q3 (July-September 2011, monsoon clouds) and Q4 (October-December 2011, winter frontal systems).

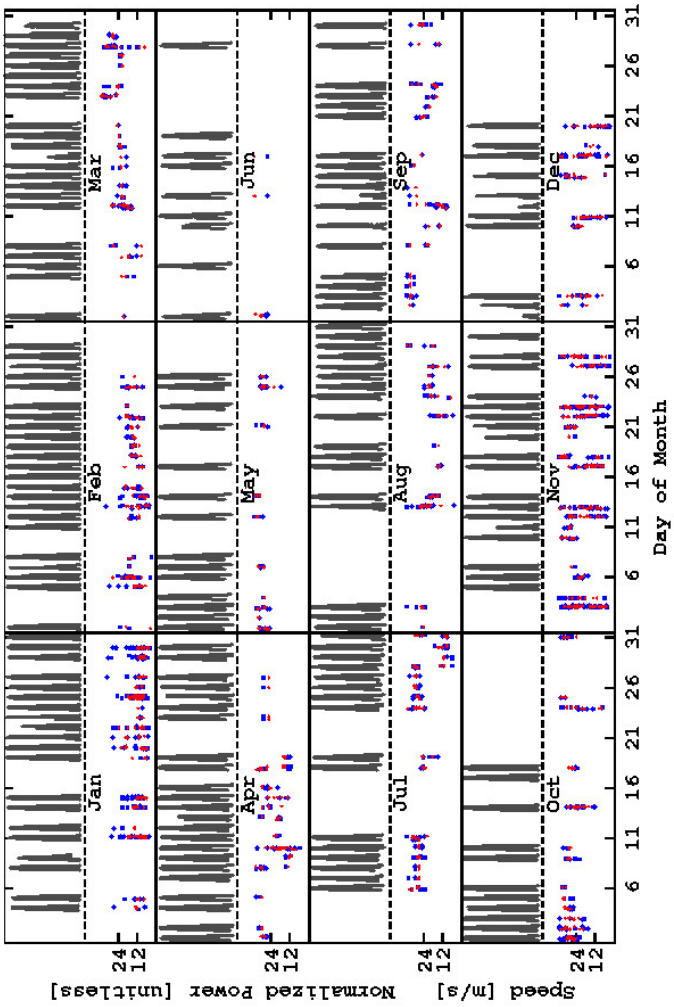

Fig. 4 LCE (blue) and MCC (red) cloud speed results for the whole studied year.

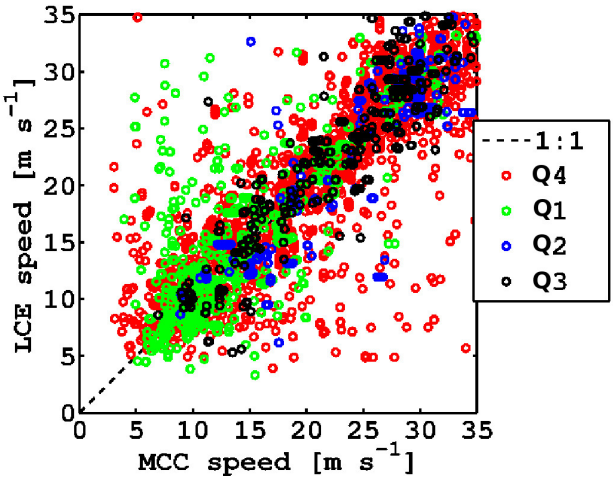

Fig.5 LCE vs MCC results scatter plot.

A total of 2700 cloud speeds from both the LCE and MCC methods were compared in terms of Root Mean Squared Error (RMSE) and Mean Bias Error (MBE) where the CCM cloud speed is considered as the ground truth and the errors are calculated as a percentage of the mean MCC speed value. Fig. 4 shows the cloud speeds from the LCE and MCC methods and normalized power output from the inverters. It can be observed that CMVs are detected during the whole year, with the highest number of completely clear days during June, October and December. Some of the days were some clouds were detected do not contain any resulting CMVs due to the quality control process on the resulting data. Also January and November show the largest intra-day variability. The general trend of the speeds detected by both methods follow the same yearly pattern, as observed by the errors obtained for the different quarters.

Figure 5 shows the combined scatter plot of cloud speeds in the different seasons. The largest spreads are evident for the first and fourth terms, but with an overall grouping around the 1:1 line. It is worth noting that even though the MCC results are considered the ground truth, they have been calculated from the cloud direction detected by the LCE method. According to a previous study (9) cloud directions observed from both methods are considered to be very similar, but the error propagated from this assumption will cause some of the spread observed in Fig. 5.

In addition, Table 2 show the validation of LCE results against the CCM separated by season. The average detected cloud speeds are lower for the first quarter of the year. The first quarter also registered the largest relative errors for both RMSE and MBE, showing a general trend of the LCE results to underestimate the MCC output. The second quarter shows the largest speeds and a relatively small RMSE and MBE. The third and fourth quarters show similar average cloud speeds and also a small MBE, with the overall smallest RMSE during the third quarter. The combined -0.9% MBE shows that both methodologies yield similar results even though they are based on very different concepts and data.

TABLE 2: ERROR METRICS FOR CLOUD SPEED BY SEASON INCLUDING NUMBER OF DAYS AND AVERAGE SPEEDS.

Period	Days	v_{mean} ms^{-1}	RMSE %	MBE %
Q1	66	15.0	29.3	-5.5
Q2	46	25.9	14.7	2.7
Q3	56	22.9	13.7	-1.2
Q4	58	22.5	21.8	0.7
All	226	21.6	20.9	-0.9

5. CONCLUSIONS

Encouraging CMV results are obtained from the LCE applied to data from two arbitrary triplets of reference cells when compared to the more robust cross-correlation method. The results indicate especially if only a reduced number of sensors is available, LCE is reliable option for cloud speed detection with an overall annual RMSE of 20.9%. A seasonal dependence of cloud speeds and the accuracy of detection was observed, with an optimal match of both methodologies during the July-September period yielding a 13.7% RMSE and also a low -1.2% MBE.

Future work will repeat this analysis in different areas to study the generality of the developed models, e.g. to confirm and examine the performance for lower cloud speed typical for coastal region. The application of the generated CMVs will also be used as input to short term forecast and variability algorithms to evalute whether such CMVs can lead to more accurate forecast and variability models. A more comprehensive CMV database could be assembled which is currently lacking due to the inherent difficulty of cloud speed measurements.

6. ACKNOWLEDGMENTS

This work was supported in part by the California Solar Initiative RD&D program. We also appreciate the help of David Jeon, Leslie Padilla, and Shiva Bahuman from Sempra US Gas and Power and Bryan Urquhart from UCSD for providing and supporting the Copper Mountain data.

7. REFERENCES

(1) Pelland, S., Galanis, G., Kallos, G., 2011. Solar and photovoltaic forecasting through post-processing of the Global Environmental Multiscale numerical weather prediction model. Progress in Photovoltaics: Research and Applications, http://dx.doi.org/10.1002/pip.1180

(2) Chow, C.W., Urquhart, B., Lave, M., Dominguez, A., Kleissl, J., Shields, J., Washom, B., 2011. Intra-hour forecasting with a total sky imager at the UCSan Diego solar energy testbed. Solar Energy 85, 2881-2893

(3) Perez, R., Kivalov, S., Schlemmer, J., Jr., K.H., Renné, D., Hoff, T.E., 2010. Validation of short and medium term operational solar radiation forecasts in the US. Solar Energy 84, 2161–2172

(4) Hoff, T.E., Perez, R., 2010. Quantifying PV power output variability. Solar Energy 84, 1782–1793

(5) Lave, M., Kleissl, J., 2013. Cloud speed impact on solar variability scaling - Application to the Wavelet Variability Model. Solar Energy , In Press

(6) Hammer, A., Heinemann, D., Lorenz, E., Lückehe, B., 1999. Short-term fore- casting of solar radiation: a statistical approach using satellite data. Solar Energy 67, 139–150

(7) Leese, J.A., Novak, C.S., Clark, B.B., 1971. An automated technique for obtaining cloud motion from geosynchronous satellite data using cross correlation.Journal of Applied Meteorology 10, 118–132

(8) Lorenz, E., Hammer, A., Heinemann, D., 2004. Short term forecasting of solar radiation based on satellite data. Proc. ISES Europe Solar Congress EUROSUN 2004,Freiburg, Germany, 2004

(9) Bosch, J., Zheng, Y., Kleissl, J., 2013. Deriving cloud velocity from an array of solar radiation measurements. Solar Energy 87, 196–203